Post-Contact, In-Hand Object Motion Compensation With Adaptive Hands

Minas V. Liarokapis, *Member, IEEE*, and Aaron M. Dollar, *Senior Member, IEEE*

***Abstract*— In this paper, we present a methodology based on constrained optimization methods for estimating and compensating for post-contact parasitic object motions for underactuated, compliant robot hands and for deriving stable, minimal effort grasps to try to minimize these movements. To do so, we compute the object motions for different hand designs, object shapes, and object sizes and we synthesize appropriate robot arm trajectories that eliminate them, even in hands with complex flexure-based compliant members. The effectiveness of the proposed methods is validated using a seven DOF robot arm (Barrett WAM) and a range of compliant underactuated robot hands (Yale OpenHand models T42PP, T42PF, and T42FF).**

***Note to Practitioners*—During precision fingertip grasps, adaptive hands tend to move the object upon contact, to an equilibrium configuration determined by the elasticity of the mechanism and the forces exerted on the hand-object system. Such a behavior may be undesired for certain tasks (e.g., when grasping a full glass of water, the in-hand object perturbations may spill the water). In this paper, we propose a methodology for adaptive hands that derives stable minimal effort grasps, computes the post-contact parasitic object motions, and eliminates them using compensatory motions of a robot arm.**

***Index Terms*— Adaptive hands, grasping, kinematics, manipulation, underactuated mechanisms.**

I. Introduction

ADAPTIVE, underactuated, and compliant robot hands [1]–[3] have been heavily investigated in recent years, for both robust grasping [4]–[7] and dexterous in-hand manipulation [8]–[11] (e.g., equilibrium point manipulation, flip and pinch, stick and slip, and finger gaiting). The motivation behind these efforts comes from the fact that the reduced number of actuators and constraints of these mechanisms can significantly simplify the grasping and manipulation process, relaxing at the same time the computational complexity and the required control effort. Indeed, these hands can often be reliably used for stable grasping even in an open-loop fashion and without performing any in-depth grasp synthesis (e.g., selection of appropriate contact forces or optimal contact points). However, due to the underactuation and the use of mechanical compliance, the hand-object system often reconfigures during the grasping process as force is applied.

Manuscript received April 28, 2016; revised September 23, 2016; accepted October 6, 2016. Date of publication December 21, 2016; date of current version April 5, 2018. This paper was recommended for publication by Associate Editor S. Carpin and Editor M. Wang upon evaluation of the reviewer's comments. This work was supported by NSF NRI under Grant IIS-1317976.

The authors are with the School of Engineering and Applied Science, Yale University, New Haven, CT 06511 USA (e-mail: minas.liarokapis@yale.edu; aaron.dollar@yale.edu).

Color versions of one or more of the figures in this paper are available online at http://ieeexplore.ieee.org.

Digital Object Identifier 10.1109/TASE.2016.2622001

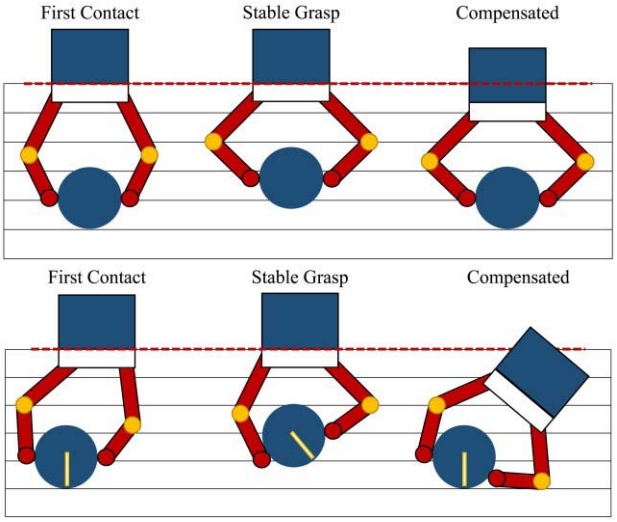

Fig. 1. Post-contact, parasitic object motion and object motion compensation examples. First row: example of a symmetrical grasp. Second row: arbitrary nonsymmetric grasp.

In this paper, we propose a complete scheme for performing grasp synthesis and post-contact, parasitic object motion compensation for adaptive hands. In particular, we derive a set of optimal contact points and forces that facilitate the execution of optimal minimal effort grasps (e.g., prior to manipulation), and lead to the minimization of both the post-contact parasitic object motion and the hand power consumption, as well as appropriate compensatory motions of the arm that eliminate the imposed parasitic object motions (see Fig. 1). The proposed scheme is based on constrained optimization methods and models that describe the kinematics of underactuated hands during grasping, even when they utilize complex flexure joints based on elastomer materials. The efficacy of the proposed methods is validated through extensive simulated and experimental paradigms with a redundant robot arm (Barrett WAM) and different adaptive robot hands of the Yale OpenHand project (models T42PP, T42PF, and T42FF). A few related studies have focused on providing stable grasps and performing grasp quality and/or force optimization for underactuated hands. In particular, Mavrogiannis *et al.* [12] presented an optimization scheme for deriving task-specific, force closure grasps for underactuated, synergistic robot hands. For doing so, they used the soft synergy model proposed by Bicchi *et al.* [13] for modeling the kinematics and the force distribution, as well as a task compatibility index [14], [15] to derive appropriate grasping postures. Ciocarlie *et al.* [16], [17], proposed constrained optimization frameworks for compliant underactuated robot hands that take advantage of a quasistatic

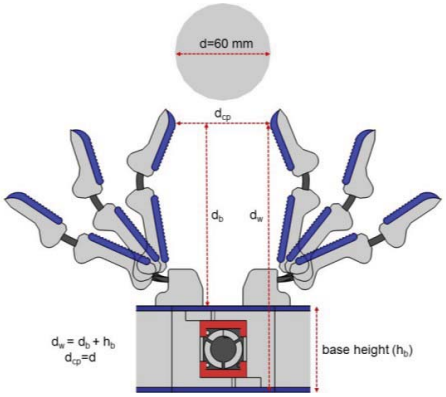

Fig. 2. Simulated paradigm of the wrist offset calculation procedure for the model T42FF of the Yale OpenHand project, reaching a sphere with a radius of 30 mm.

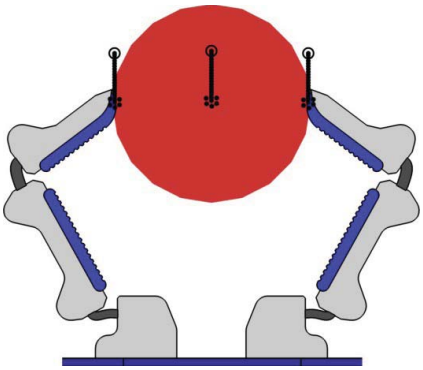

Fig. 3. Example of the parasitic motion that is imposed on the object during a pinch grasp of a sphere with a radius of 30 mm. The fingertip and object center positions are denoted with black solid (initial) and dotted (final) circles.

equilibrium formulation to find a set of design parameters that optimize stability across a set of different grasps.

However, these studies did not analyze the effect of the applied contact forces on the post-contact parasitic object motions and did not study the reconfiguration of the hand-object system. Su *et al*. [18] proposed a grasp strategy for underactuated hands that facilitates a single trial grasping (no regrasping is necessary) when there is uncertainty in the object pose. To do so, they proposed a robust grasp planning scheme that can cope with object position errors and they performed a contact/force sensors-based grasp adaptation taking into consideration in their analysis the compliant characteristics of the underactuated mechanism. Chen *et al*. [19] presented an adaptive/compliant reach-to-grasp strategy for multifingered robot hands, in order to improve their grasping performance under object pose uncertainties. This paper utilizes a spatial virtual spring framework, in order to formulate an adaptive grasping control methodology that achieves local adjustments of the robot fingers without resorting to the arm motion. Prattichizzo *et al*. [20] proposed an object motion-decoupled internal force controller for stable grasping with compliant multifingered hands, while Malvezzi *et al*. [21] proposed an internal forces controller that guarantees zero motion of the object. These studies focused only on deriving stable grasps and eliminating object motions for compliant robot hands without dealing with underactuated pinch grasps, without considering the post-contact parasitic object motion and the reconfiguration of the hand-object system, and without using the whole arm-hand system to compensate for these motions. Finally, in [22], we presented preliminary results on estimating and compensating for post-contact in-hand parasitic object motions of symmetric grasps.

The remainder of this paper is organized as follows. Section II focuses on the grasp synthesis and post-contact parasitic object motion estimation methods, analyzing how we can derive stable, minimal effort grasps and how we can compute appropriate robot arm trajectories that accurately eliminate the parasitic object motions. Section III presents the simulated and the experimental paradigms prepared with a redundant robot arm (Barrett WAM) and various adaptive, compliant, and underactuated robot hands designed within the Yale OpenHand project, while Section IV concludes this paper and discusses the future directions.

II. Methods

In this section, we present the reconfiguration estimation and the post-contact parasitic object motion compensation methods.

A. Prepositioning the Robot Arm End-Effector

To secure a stable, minimal effort grasp we need to preposition the robot arm end-effector appropriately, for the robot hand to be able to optimally grasp the desired object with the fingertips. Given the fact that we want our grasp to be as robust as possible, we choose during the grasp planning process to optimize a specific grasp quality metric [14]. The chosen metric for the simple hands examined is the distance between the contact ($\mathbf{c}_c$) and the object geometric centroid ($\mathbf{c}_g$) (used also in [22] and [23]), which is given as

$$Q_{\mathrm{DC}} = \|\mathbf{c}_c - \mathbf{c}_g\|. \tag{1}$$

To reach the desired contact points, we start closing the robot fingers by applying an increasing load at the individual finger motors, until the distance between the two fingertip positions equals a dimension of the object (e.g., the diameter of a sphere or a side of a cube). In order to compute the kinematics of the fingers in the plane relatively to the motor loads, we use the smooth curvature model [24] that provides accurate forward kinematic (FK) estimations.

Upon computing the configurations of the fingers at which the distance between the fingertips equals an object dimension, we can compute the distance from the contact points to the base frame of the hand (arm wrist), which is also the offset that the robot arm wrist should have from the object to accordingly preposition the hand and allow it to reach the desired contact points. A simulated paradigm of the proposed method is presented in Fig. 2. An example of post-contact parasitic object motion is presented in Fig. 3, for the case of model T42FF while grasping a sphere.

It must be noted that we need to preposition the hand for it to reach the desired contact points, because the underactuation of the examined hand designs restricts the motion of their fingertips in specific submanifolds of the 2-D space, limiting the feasible configurations.

Moreover, in this paper we hypothesize that we have an analytical description of both the robot and the object structures (3-D models), as well as knowledge of the object

properties (e.g., weight, stiffness, and friction between the fingertips and the object surface). The object shape and pose information can be easily derived using appropriate vision schemes. Such knowledge allows us to solve at each instance of the grasping process the FK of the hand and detect contact with the object surface, halting the corresponding finger motor. Upon contact, the loads of the motors are partially transformed into contact forces.

B. Grasp Stability

According to the grasping literature, a grasp is considered as stable if it satisfies the force closure property [25]. The force closure has two different conditions: the object should be in equilibrium and the friction cone constraints should be satisfied. The balance equation for generalized forces acting on the object, is given as

$$\mathbf{G}\mathbf{f} = -\mathbf{f}_{\text{ext}} \tag{2}$$

where $\mathbf{f}$ is the vector of the contact forces, $\mathbf{G} \in \Re^{6\times mn_c}$ is the grasp matrix, $\mathbf{f}_{\text{ext}}$ is the external wrench applied at the object center of mass, m is the dimensionality of the contact model ($m = 3$ for the Hard Finger (HF) model [12]), and n_c is the number of contact points. The general solution to the grasping force distribution problem is derived using a force decomposition model for compliant hands [26]. Such a model is given as

$$\mathbf{f} = \mathbf{G}^{+}(-\mathbf{f}_{\text{ext}}) + (\mathbf{I} - \mathbf{G}^{+}\mathbf{G})(\mathbf{K}_s \Delta\mathbf{p} + \mathbf{K}_c \delta\mathbf{p}) \tag{3}$$

where $\mathbf{K}_s = (\mathbf{C}_s + \mathbf{J}_h\mathbf{C}_q\mathbf{J}_h^T)^{-1}$ is the stiffness matrix that represents the structure compliance of the hand [27], $\mathbf{K}_c$ is the stiffness matrix of the contact points, $\mathbf{J}_h$ is the hand Jacobian, $\mathbf{C}_s$ is the diagonal matrix of the finger-pads and links compliance, $\mathbf{C}_q$ is the diagonal matrix representing the joints compliance, $\Delta\mathbf{p}$ are the virtual displacements of the fingertips that are caused by the finger joint displacements, $\delta\mathbf{p}$ are the infinitesimal deformations of the object at the contact points that depend on the object stiffness, and $\mathbf{G}^{+} = \mathbf{K}_s\mathbf{G}^T(\mathbf{G}\mathbf{K}_s\mathbf{G}^T)^{-1}$ denotes the $\mathbf{K}_s$ weighted right inverse of the grasp matrix that minimizes the potential energy

$$\frac{1}{2}\delta\mathbf{p}^T\mathbf{K}_s\delta\mathbf{p}. \tag{4}$$

The finger displacements and the object deformations at the contact points can be easily predicted by the smooth curvature model [24]. Regarding contact modeling, in this paper we use the HF model, which imposes for the "friction cone" constraints the following nonlinear inequalities:

$$\sqrt{f_{o_i}^2 + f_{t_i}^2} \le \mu f_{n_i}, \quad i = 1, \ldots, n_c \tag{5}$$

where μ is the friction coefficient, f_n is the normal force component, f_t and f_o are the tangential/shear components of the contact forces, and n_c is the number of the contact points. The normal forces are constrained to be nonnegative. The friction coefficient chosen for this study is $\mu = 0.3$ (for contacts between the finger-pads urethane rubber and the objects ABS). The friction coefficient typically ranges between 0.1 and 1 [25].

C. Grasping Force Optimization

Typically, when the object weight is unknown the user of an adaptive, underactuated, compliant hand may control it in an on–off fashion, squeezing the object arbitrarily tight, without crushing the object and without damaging the fingers (e.g., due to the underactuation and the mechanical adaptability of the design). However, this approach is not optimal for two main reasons: 1) it maximizes the post-contact parasitic object motion that is caused by the hand-object system reconfiguration and 2) it maximizes the power consumption, as arbitrarily high contact forces require higher actuator loads.

Thus, in case the object weight is known, a grasping force optimization can be employed to minimize the levels of contact forces that should be exerted through the robot fingertips and to achieve stable, minimal effort grasps. In this paper, we choose to minimize the norm of the normal contact force components, which is given as

$$F(\boldsymbol{\tau}) = \sqrt{\sum_{i=0}^{n_c} f_{n_i}^2}. \tag{6}$$

Such a minimization combined with the satisfaction of the friction cone, the joint limits, the object penetration, and the self-collision constraints leads to the minimization of the contact force distribution and therefore to an optimal, minimal effort grasp configuration. Thus, the grasping force optimization problem is formulated as follows:

$$\boldsymbol{\tau}^* = \arg\min_{\boldsymbol{\tau}} F(\boldsymbol{\tau}) \tag{7}$$

s.t.

$$\sqrt{f_{o_i}^2 + f_{t_i}^2} \le \mu f_{n_i}, i = 1, \ldots, n_c \tag{8}$$

$$\mathbf{q}^- \le \mathbf{q} \le \mathbf{q}^+ \tag{9}$$

$$\mathbf{c}_i \in \partial O, i = 1, \ldots, n_c \tag{10}$$

$$S_h \notin O \tag{11}$$

$$(C_l \cap C_{l-1}) \cup (C_l \cap C_{l-2}) \ldots (C_2 \cap C_1) = \emptyset, \quad l = 1, \ldots, n_l \tag{12}$$

where τ denotes the generalized forces acting on the system, $\mathbf{q}^-$ and $\mathbf{q}^+$ denote the lower and the upper joint limits, O is the space occupied by the object, $\mathbf{x}_{cp_i}$ is a vector containing the coordinates of the ith fingertip of the robot hand that must lie on the object surface ∂O as described in (10), S_h is a set of finite discrete points lying on the robot hand links (i.e., rigid phalanges) that should not penetrate the object, l is the number of links per finger, and C_l is the convex hull of the 3-D mesh points of the lth phalange. The intersection of these convex hulls should always be $\emptyset$ to avoid intrafinger collisions, like the one depicted in Fig. 4.

In the case of elastic pin joints, the intrafinger collisions can also be represented with much simpler inequality constraints as in (9). In the case of flexures, such simple joint limits are hard to be defined, thus we use (12). It should be noted that (10) and (11) require an analytical description of the object geometry. For the simple case of an object that has a primitive shape (e.g., a cylinder) (10) and (11) can be represented by a series of inequality constraints. In the rest of this paper,

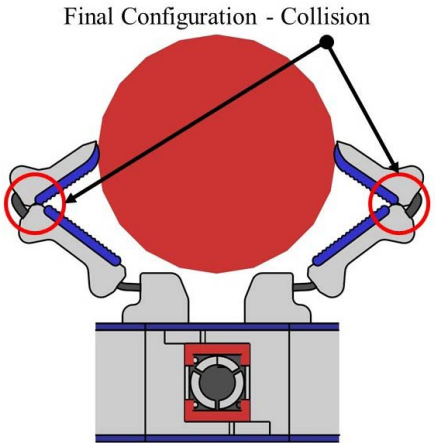

Fig. 4. Reconfiguration of the hand-object system is interrupted by a collision between the proximal and the distal phalanges of each finger.

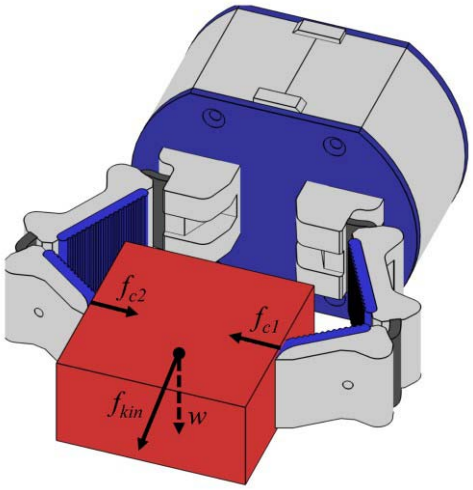

Fig. 5. Forces acting on the hand-object system. The contact points are denoted by f_{c1} and f_{c2}, f_{kin} is the force of the kinetic friction, and w is the weight of the object. The simulated hand is the model T42FF that has two flexure joints per finger and the object grasped is a rectangle with a side of 60 mm.

we denote all these constraints with the abbreviation *RHC* (robot hand constraints).

D. Joint Elasticity

In this section, we describe the modeling process for adaptive robot hands with spring loaded pin joints as well as for adaptive hands implemented with flexure joints based on elastomer materials. For the case of simple elastic pin joints, the configuration of the hand at equilibrium is found by minimizing the energy of the hand-object system. The potential energy of the hand is expressed as follows:

$$V(\mathbf{q}) = \frac{1}{2}\mathbf{q}^T\mathbf{K}\mathbf{q} \tag{13}$$

where $\mathbf{q}$ is the vector of the joint angles and $\mathbf{K}$ is the stiffness matrix that represents the pin joint compliances. For the case of flexure joints, the smooth curvature model [24], [28] can be used. The particular model provides estimations of the kinematics of robots equipped with planar flexure joints and is based on the assumption that the curvature of elastic beams during bending is smooth and can be approximated by low-order polynomials. The flexure joint bending is described with three generalized coordinates instead of one that is used for the pin joints. The proposed model provides a set of homogeneous transformations between the robot rigid links, as well as the derivatives of the kinematics (e.g., Jacobian and Hessian matrices).

Once again the configuration of the hand-object system at equilibrium is found via a minimization of the potential energy of the system $V(\boldsymbol{q})$, as reported in [24]. Using the smooth curvature model, we can derive the finger poses relatively to the tendon displacements or the tendon loads, as well as to accurately represent the effect of any external forces acting on the robot structure. An example of external force acting on the system is the kinetic friction force that depends on the object weight and the friction between the object surface and the environment. The problem is formulated as a constrained energy minimization.

More precisely, let τ denote the generalized forces acting on the system, $\mathbf{f}$ the vector of the forces applied at a specific point $\mathbf{p}$ on the robot (e.g., contact points), $\mathbf{J}_p^T$ be the Jacobian of the particular point coordinates, and $\nabla_q V$ the gradient of the total internal energy of the robot. Then, the equilibrium configuration of the hand-object system can be found by minimizing the following function:

$$E(\tau) = -\nabla_q V(\mathbf{q}) + \mathbf{J}_p^T\mathbf{f}. \tag{14}$$

It must be noted that the vector of forces $\mathbf{f}$ incorporates also the effect of friction between the grasped object and the supporting surface. More precisely, the force of kinetic friction is a reaction force that depends upon the magnitude of the "pulling force" of the reconfiguring hand-object system that pushes the object along the table surface and typically within the grasp (see Fig. 5).

At this point, we would like to distinguish between three types of contact forces that can be exerted by the robot fingertips. These forces are as follows:

1) $\mathbf{f_{min}}$: The minimum contact forces required to achieve a minimal effort grasp, given the object weight;
2) $\mathbf{f_e}$: The minimum contact forces required in order for the hand-object system to reach an equilibrium configuration at which the reconfiguration stops;
3) $\mathbf{f_{max}}$: The maximum contact forces that can be exerted on the object and that are mainly bounded by the torque limits of the finger actuators\motors.

The relationship between these forces is typically given as

$$\mathbf{f_{min}} < \mathbf{f_e} < \mathbf{f_{max}}. \tag{15}$$

It must be noted that the set of forces $\mathbf{f_e}$ leads to a hand-object system configuration where the system is no longer underconstrained and at which the loads of the motors are partially transformed into equivalent contact forces at the contact points. At this configuration, no additional reconfiguration of the object/object system is possible.

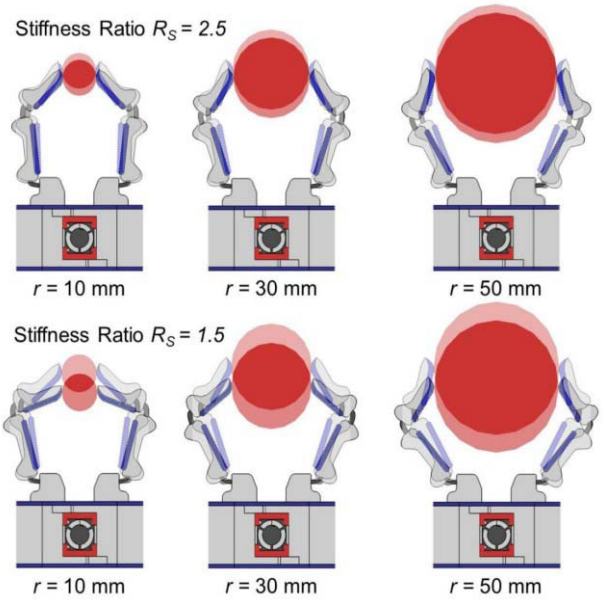

Fig. 6. Simulated paradigms of the post-contact reconfiguration and of the imposed parasitic object motion for robot hands with various stiffness ratios $R_S = S_D/S_P$, between the distal (S_D) and the proximal phalanges (S_P). Different stiffness ratios result in different total reconfigurations of the fingers and, consequently, in different object displacements. The simulated objects used are spheres with radii 10, 30, and 50 mm, respectively. The initial and the final configurations appear superimposed to facilitate comparison.

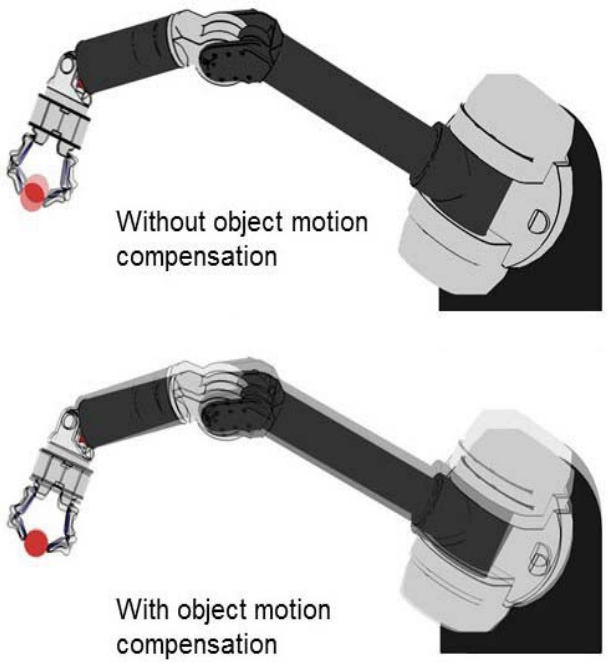

Fig. 7. Simulated paradigm of the parasitic object motion compensation procedure using the Barrett WAM—-Yale OpenHand model T42 robot arm-hand system. The examined task involves grasping of a sphere with a radius of 20 mm. A compensatory motion of the arm can eliminate the parasitic object motion, securing a stable grasp. The initial and the final configurations of the arm-hand system appear superimposed to facilitate comparison.

E. Parasitic Object Motion Estimation

As we have already noted in the previous sections, in this paper we have complete knowledge of the object parameters. Thus, we can derive a set of minimal contact forces that will result in a stable, minimal effort grasp of the examined object. Such grasps are quite valuable for a series of applications, as they lead to minimal power consumption of the system (e.g., important for UAVs that rely on the same battery for operating both their motors and a gripper) and to minimal post-contact, parasitic object displacements.

Upon deriving a set of contact forces, we are able to predict the object motion and the imposed reconfiguration of the underactuated robot fingers, using (14) and the smooth curvature model [24], as described in [29]. The forces acting upon the system are the motor loads, the contact forces exerted on the object, and the resisting force imposed by the friction between the object and the supporting surface. These forces trigger a reconfiguration of the underactuated compliant robot fingers, which leads the hand-object system to an elastic equilibrium configuration.

Thus, the problem of deriving the post-contact parasitic object motion for the case of adaptive, underactuated, and compliant robot hands, can be formulated as

$$\boldsymbol{\tau}^* = \arg\min_{\boldsymbol{\tau}} E(\boldsymbol{\tau}) \quad \text{s.t.} \quad RHC \tag{16}$$

where *RHC* are the robot hand constraints described in (8)–(12). The velocity of the object is extracted from the robot fingertip velocities using the grasp matrix $\mathbf{G}$. It should be noted that in the case of nonsymmetrical grasps, there is a coupled rotation and translation in the parasitic object motion that requires a significantly more complex compensatory motion of the robot arm. This coupled rotation and translation is caused by the unbalanced fingertip contact forces and the nonsymmetric contact rolling between the two fingers and the object.

In Fig. 6, we present various examples of post-contact parasitic object motion estimation using simulated models of the examined adaptive robot hands with different parameters. More precisely, the examples concern a series of simulated model T42FF underactuated robot hands with different stiffness ratios between the proximal and the distal joints. The hands are depicted while grasping and they are imposing parasitic object displacements to spheres with radii of 10, 20, 30 40, and 50 mm. Different stiffness ratios lead to different elastic equilibrium configurations and thus to different post-contact, parasitic object motions.

F. Deriving Compensatory Robot Arm Motion

Having estimated the parasitic object motion, we can easily derive an appropriate compensatory motion of the robot arm (wrist) end-effector, using the robot arm Jacobian $\mathbf{J}_a$. To eliminate the parasitic object motion, we need the robot arm end-effector velocity to have equal but of opposite direction velocity with the object, at each time instance of the grasping process (see Fig. 7). Let $\mathbf{v}_{ee}$ be the desired velocity of the robot arm end-effector. Then, we can derive the arm joint space velocities that are given as

$$\dot{\mathbf{q}} = \mathbf{J}_a^{+}\mathbf{v}_{ee} \tag{17}$$

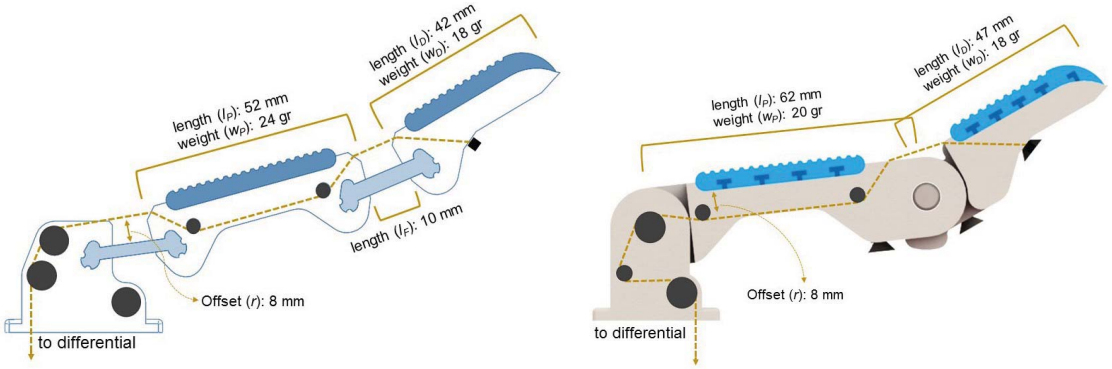

Fig. 8. Exemplar finger structures of the models T42FF (left) and T42PP (right).

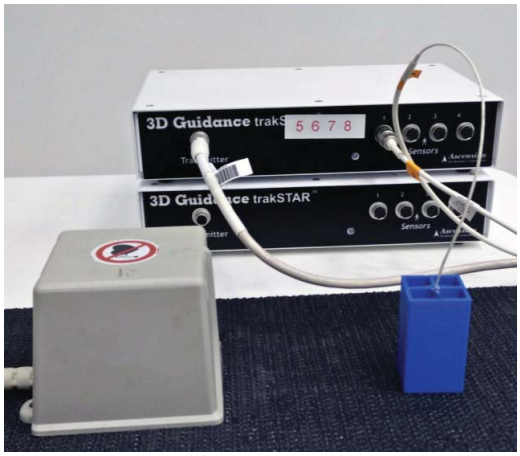

Fig. 9. TrakSTAR (Ascension Technologies) magnetic motion capture system and a rectangular sensorized, 3-D printed, rectangular object. The trakSTAR system is equipped with an MRT and 8 model-180 magnetic sensors that have a diameter of 2 mm. In this paper, we use a single sensor to capture the pose of the examined objects.

where $\mathbf{J}_a^+$ is the robot arm pseudoinverse (in this paper we use a redundant seven DoF robot arm), which is given by the following expression:

$$\mathbf{J}_a^+ = \mathbf{J}_a^T(\mathbf{J}_a\mathbf{J}_a^T)^{-1}. \tag{18}$$

An appropriate motion of the whole arm-hand system can successfully compensate for the parasitic object motion. More results for both symmetric and nonsymmetric grasps are presented in the following section.

III. Results and Experiments

In this section, we present both the simulated and the experimental paradigms prepared with the Barrett WAM robot arm and the compliant underactuated robot hands. For the computation of the kinematics of the underactuated robot hands, we used the freeform manipulator toolbox [24], the SynGrasp toolbox [30], and the Robotics Toolbox [31] in the MATLAB (MathWorks) interactive simulation environment.

A. Apparatus

In this paper, we use the seven DoF Barrett WAM robot arm [32] and different adaptive robot hands of the Yale OpenHand project. The hands are the models T42PP, T42FF, and T42PF. Model T42 is an open-source, two-fingered, compliant, underactuated, tendon-driven robot hand that has two motors (a dedicated motor for each one of the two robot fingers) and two phalanges per finger.

TABLE I
Yale OpenHand Model T42 Robot Hands Properties

Model T42 FF	
Parameters:	**Values:**
Distal phalanx length (l_D)	0.042 m
Proximal phalanx length (l_P)	0.052 m
Flexure joint length (l_F)	0.010 m
Tendon routing offset (r)	0.008 m
Distal phalanx weight (w_D)	0.018 kg
Proximal phalanx weight (w_P)	0.024 kg
Model T42 PF	
Parameters:	**Values:**
Distal phalanx length (l_D)	0.042 m
Proximal phalanx length (l_P)	0.058 m
Flexure joint length (l_F)	0.010 m
Tendon routing offset (r)	0.008 m
Distal phalanx weight (w_D)	0.018 kg
Proximal phalanx weight (w_P)	0.023 kg
Model T42 PP	
Parameters:	**Values:**
Distal phalanx length (l_D)	0.047 m
Proximal phalanx length (l_P)	0.062 m
Tendon routing offset (r)	0.008 m
Distal phalanx weight (w_D)	0.018 kg
Proximal phalanx weight (w_P)	0.020 kg

The flexure joints of models FF and PF are implemented with elastomer materials (Smooth-On, PMC 780 Urethane Rubber). More details regarding the examined robot hands and all the required instructions for their replication can be found in the Yale OpenHand project website [33]. The T42 parameters are reported in Table I and the tendon routing as well as the structures of exemplar fingers are depicted in Fig. 8. All the models of the robot arms and hands were incorporated in MATLAB for preparing a series of simulated paradigms.

To track the motion of the examined objects during the reconfiguration of the hand-object system, we used the trakSTAR (Ascension Technologies) magnetic motion capture system, which is equipped with a medium range transmitter (MRT) and 8 model-180 magnetic sensors with a

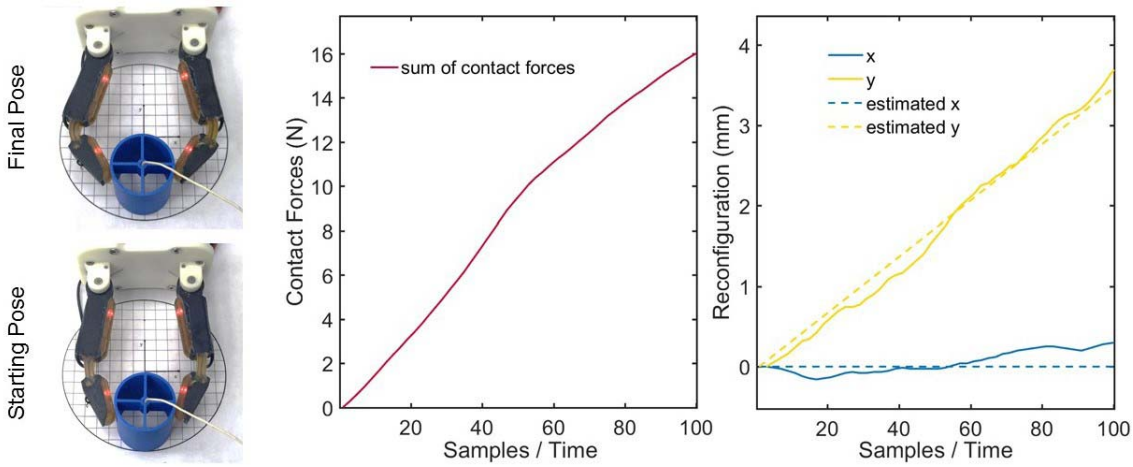

Fig. 10. The sum of the contact forces, the predicted parasitic object motion, and the actual parasitic object motion for a symmetric pinch grasp of a 3-D printed cylinder with a diameter of 45 mm. The robot hand used is a modified version of the T42PF that has 8 tactile sensors (Takkstrip, RightHand Robotics) per finger. The fingers are similar to the ReFlex hand fingers [38].

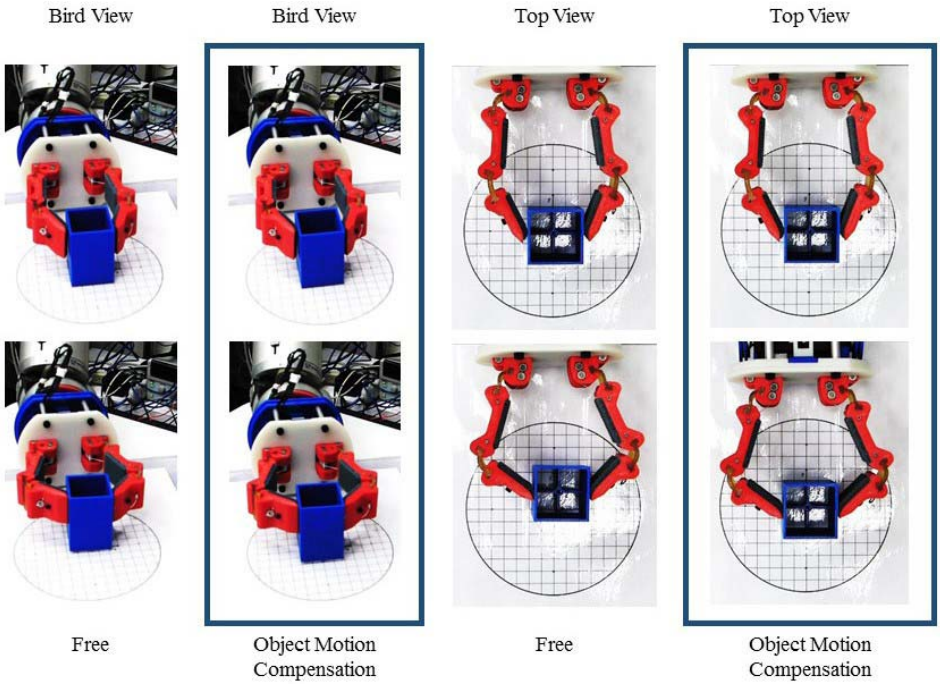

Fig. 11. Images of the symmetric grasp experiments that were conducted with the Barrett WAM—-Yale OpenHand model T42FF robot arm-hand system. The object examined is a rectangle with a side of 40 mm, which is grasped with and without the parasitic object motion compensation methodology.

diameter of 2 mm (see Fig. 9). The trakSTAR system provides high accuracy in both position and orientation with 1.4 mm and 0.5°, respectively. The sampling rate is 80 Hz and the measurements can be provided in terms of homogeneous transformation matrices.

B. Parasitic Object Motion Estimation

In Fig. 10, we present the sum of the contact forces, the predicted parasitic object motion, and the actual parasitic object motion for a symmetric pinch grasp of a 3-D printed cylinder with a diameter of 45 mm. The robot hand used is a modified version of the T42PF with 8 tactile sensors (Takkstrip [34], RightHand Robotics) incorporated in each finger. To compare the actual and the predicted parasitic object motion, quantify their similarity, and express it as a percentage, we used as a metric the percentage of the normalized mean-square error. For the experiment presented in Fig. 10, the estimated post-contact parasitic object motion is a pure translation in the y-axis, while the predicted x-axis displacement is zero. The actual parasitic object motion differs from the theoretical due to friction phenomena and/or design asymmetries in the robot hand structure. The similarity score in the y-axis is 96.4%, the maximum error is 0.23 mm, while the maximum error in the object pose displacement estimation in the x-axis is 0.50 mm.

An experimental paradigm of the Barrett WAM—model T42FF robot arm-hand system grasping a rectangle with and without the object motion compensation and with a symmetric grasp is shown in Fig. 11. Columns 1 and 3 in Fig. 11 present the initial and final configurations of the post-contact parasitic

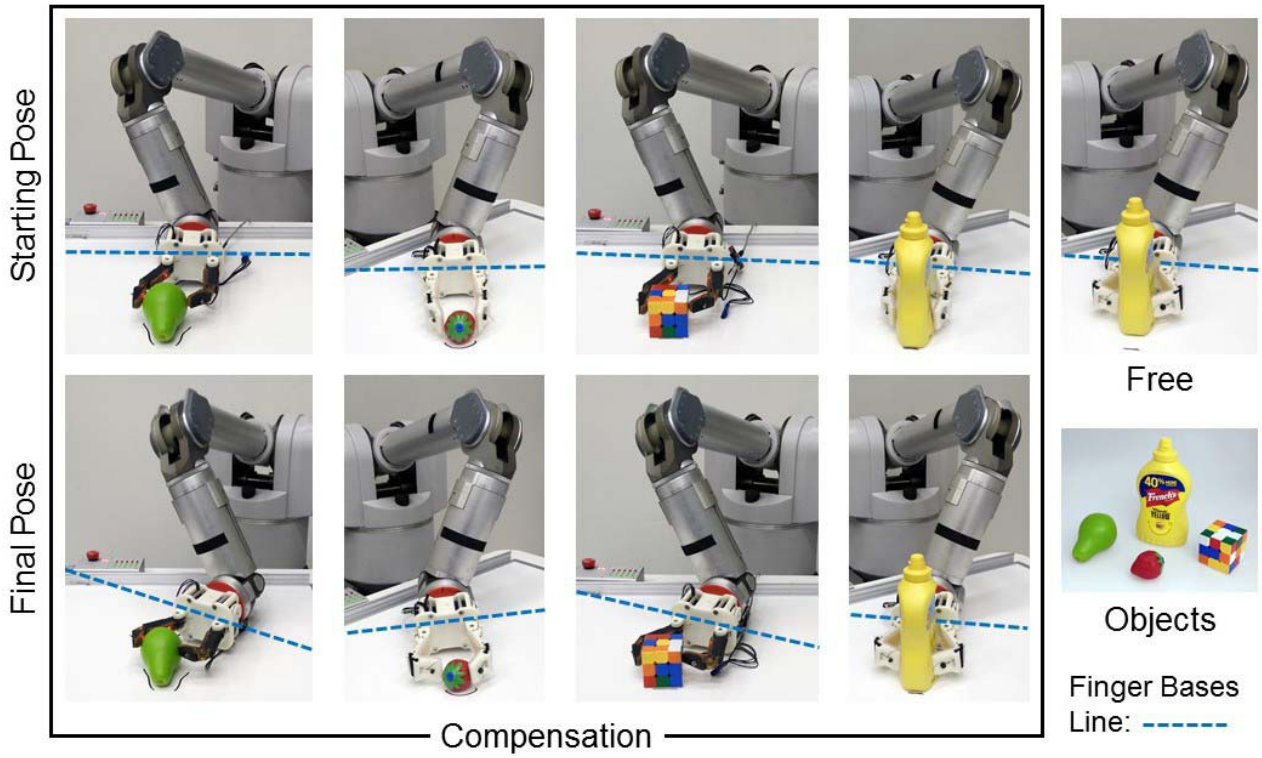

Fig. 12. Experiments of post-contact, parasitic object motion compensation for grasps of everyday life objects. The objects considered are a plastic pear, a plastic strawberry, a Rubik's cube, and a bottle of mustard and they are approximated as primitive shapes. All the objects can be found in the YCB object set [35]. The experiments were conducted with two different versions of the model T42PF robot hand.

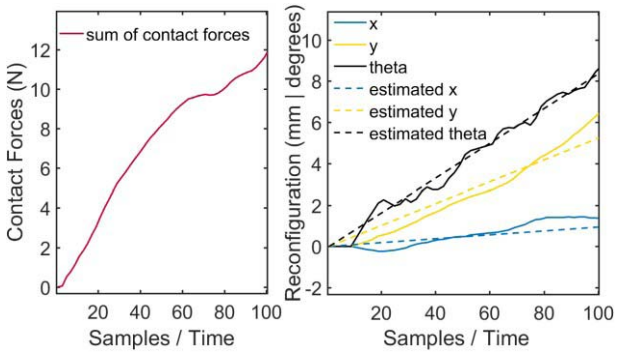

Fig. 13. Sum of the contact forces, predicted parasitic object motion, and actual parasitic object motion for a nonsymmetric pinch grasp of a bottle of mustard. The object is included in the YCB object set [35]. The mean estimation accuracy for x, y, and θ is 89.34%. The maximum errors in x, y, and θ are 0.42 mm, 0.55 mm, and 0.67°, respectively.

TABLE II
ESTIMATION ACCURACY OF THE PARASITIC OBJECT MOTION ESTIMATION FOR DIFFERENT HANDS, GRASPS, AND EVERYDAY LIFE OBJECTS

Hand	Object	Accuracy
T42PF with tactile sensors	Non-symmetric grasp of a plastic pear.	86.49%
	Non-symmetric grasp of a Rubik's Cube	95.25%
Standard T42PF	Non-symmetric grasp of a plastic strawberry.	92.14%
	Symmetric grasp of a mustard bottle.	96.53%

object motion without compensation, while columns 2 and 4 present the initial and the final configuration of the hand-object system for the object motion compensation case.

Experiments with everyday life objects are presented in Fig. 12. The objects considered are a plastic pear, a plastic strawberry, a Rubik's cube, and a bottle of mustard that can be found in the YCB object set [35]. The hands used are two different versions of the model T42PF, a standard hand, and a hand with thinner fingers that are equipped with tactile sensors and that have stiffer joints. Although we do not have an accurate description of the everyday life objects 3-D models we can approximate them with primitive shapes (e.g., cylinders, spheres, rectangles) of equal dimensions. The accuracy of the estimations of the proposed methodology for the pinch grasps with everyday life objects that we presented in Fig. 12 can be found in Table II.

Fig. 13 provides the sum of the contact forces, as well as the predicted and the actual parasitic object motions for a nonsymmetric grasp of a bottle of mustard. In this case, the estimation accuracy is only 89.34% in contrast to the 96.53% achieved for the symmetric case. This is due to the increased complexity of the post-contact parasitic object motions for nonsymmetric grasps and to the approximation of the bottle of mustard as a simple rectangle.

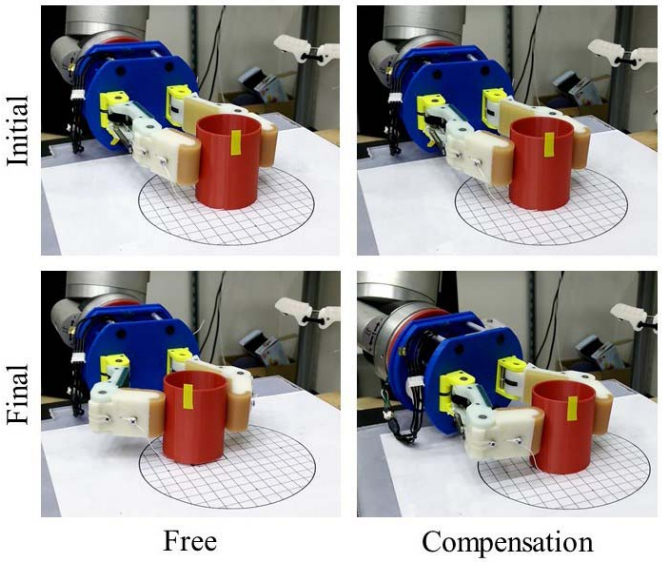

Fig. 14. Images of the nonsymmetric grasp experiments that were conducted with the model T42PP robot hand. The object examined is a 3-D printed cylinder with a diameter of 40 mm that was grasped with and without the parasitic object motion compensation. The yellow marker is used to facilitate the comparison between the "free" and the "compensation" case. It is evident that for nonsymmetric grasps, the post-contact parasitic object motion has both a translational and a rotational component. For the robot arm to compensate for this complex object motion an appropriate combination of translation and reorientation of the robot wrist is required. The similarity score for this experiment was 94.8%.

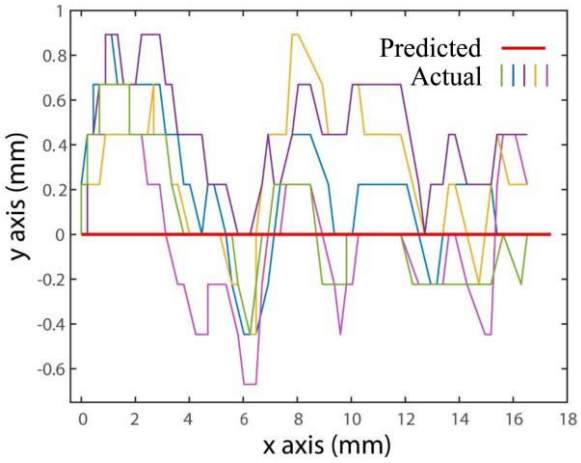

Fig. 15. Comparison of the predicted (thick red line) and the actual (thin colored lines) post-contact, parasitic object motions imposed by the reconfiguration of the hand-object system. Five different trials with the model T42PF grasping a cylinder (d: 30 mm) with a symmetrical grasp are depicted. The actual experimental data deviate from the "theoretical" object motion, due to friction terms that cannot be easily modeled (e.g., tendon routing friction and capstan effect) and modeling inaccuracies (e.g., joint compliance errors).

As it can be noticed, the parasitic object motion estimations for the everyday life objects and the nonsymmetric grasps are less accurate but the methodology still manages to compensate for the imposed object displacements and it provides a reasonable performance. It should also be noted that hands with stiffer joints (e.g., the T42PF version with the tactile sensors) produce less parasitic object motion and they can be modeled more accurately, as their behavior is not easily affected by friction phenomena.

In Fig. 14, the Barrett WAM–model T42PP robot arm-hand system grasps a cylinder with a diameter of 40 mm with and without the object motion compensation and with a nonsymmetric grasp. The parasitic motion of the object includes both a translation and a rotation component. The yellow marker is used to highlight the orientation changes.

It is evident that the proposed methodology works efficiently for both symmetrical and nonsymmetrical grasps. Upon contact of the fingertips with the object surface, there is a significant parasitic reconfiguration of the hand-object system in all the cases. Using the proposed procedure, the object displacement is eliminated by an appropriate compensatory motion of the robot arm that may involve a simple translation (symmetric grasp) or a combination of translation and rotation components (nonsymmetric grasp). The accuracy of the estimations is high in all the cases even for nonsymmetric grasps and the similarity between the estimated and the actual motion ranges between 86% and 97%, as reported in Table II.

It should also be noted that the proposed methodology cannot be 100% accurate as it does not incorporate difficult-to-model friction phenomena that take place in the finger structure (e.g., tendon routing friction and capstan effect [36]) and it does not take into consideration possible asymmetries in the robot hand structure (e.g., caused by inaccuracies in the tendon termination). Despite the missing terms, the accuracy of the proposed approach is quite promising.

Further results are depicted in Fig. 15, where the actual and the predicted post-contact parasitic object motions are compared. As expected, the predicted (theoretical) object trajectory for a symmetric grasp is a straight line. In reality, the friction phenomena in the hand structure (e.g., tendon routing friction) and other modeling inaccuracies (e.g., joint stiffness modeling inaccuracies) will always lead to object trajectories that deviate from the theoretical behavior. Though, it should be noted that the mean RMS error across all the trials in the object trajectory is only 0.4 mm for a total object displacement of ∼16 mm. It can also be noticed that the actual object trajectories are longer than the predicted trajectories.

C. Effect of Kinetic Friction Force

To investigate the effect of the kinetic friction force in the reconfiguration magnitude, we conducted multiple experiments involving 3-D printed model objects (cylinders that are filled with calibrated weights) and everyday life objects (a heavy bottle of mustard with a weight of 600 g and a plastic strawberry with a weight of 18 g) using the same robot hand. Images of the first experiment as well as the magnitudes of the post-contact parasitic object motions for the different cases are presented in Fig. 16. As can be noticed, when the object weight increases the reconfiguration magnitude decreases, as the kinetic friction force resists the reconfiguration. We should also clarify that we chose to vary the kinetic friction force by altering the object weight, because it is technically challenging to vary the level of friction between the object and the resting surface (e.g., a table).

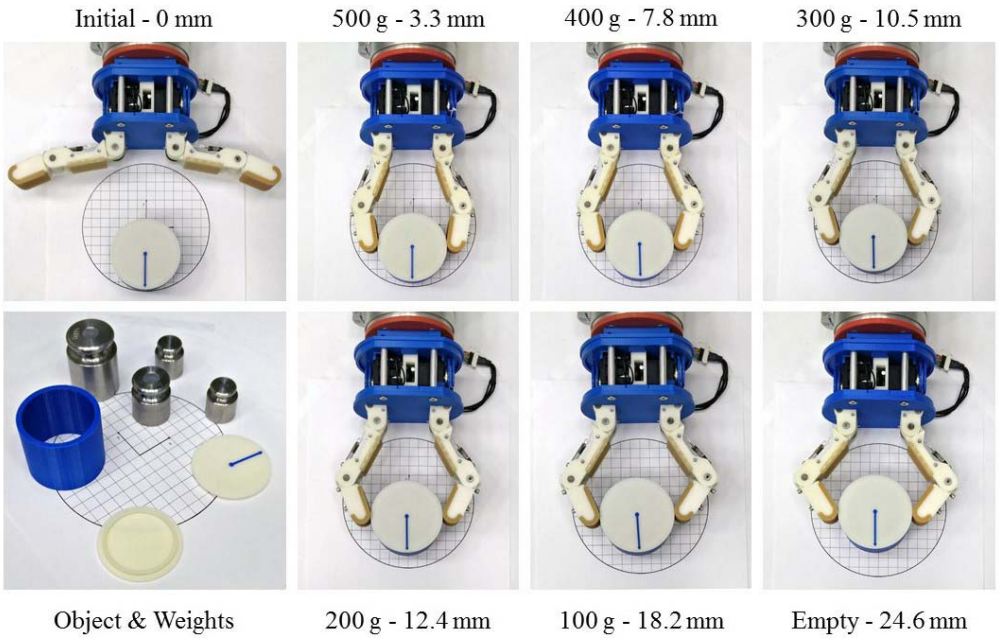

Fig. 16. Effect of the kinetic friction force in the post-contact parasitic object motion magnitude. When we change the weight of the grasped object, the kinetic friction force increases and the reconfiguration magnitude decreases (for fixed contact forces). In order to increase the weight, we use a set of calibrated weights that are incorporated in appropriately designed 3-D printed hollow objects. The weights (g) and the magnitude of the reconfiguration (mm) are also depicted.

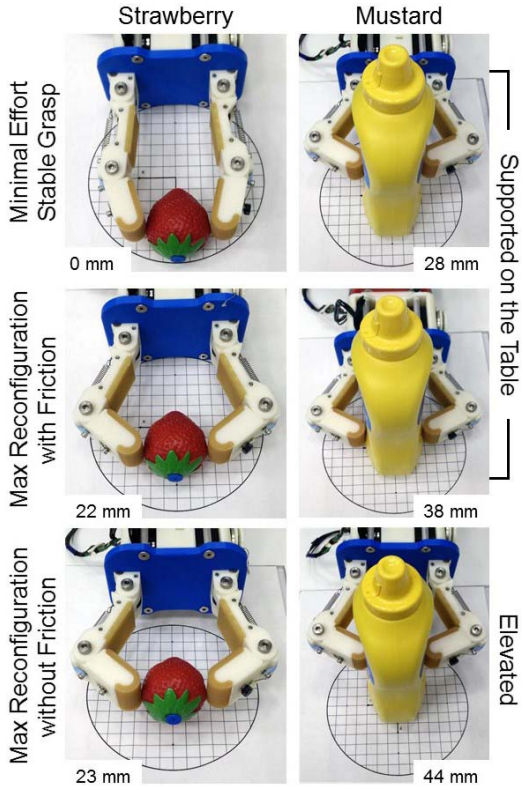

Fig. 17. Symmetric pinch grasps of a lightweight object (plastic strawberry) and a heavy object (bottle of mustard). First row: minimal effort stable grasps. Second and third rows: maximum reconfiguration poses with friction (the object lies on the table) and without friction (the object is elevated). White boxes contain the values of the magnitude of reconfiguration.

Instances of the second experiment are presented in Fig. 17. The first row in Fig. 17 depicts the minimal effort, stable grasps for two everyday life objects. The forces required to stably grasp the plastic strawberry do not impose a parasitic object motion, while the contact forces required to stably grasp the bottle of mustard impose a pure translation of the object of 28 mm. The second and the third rows in Fig. 17 present the maximum reconfiguration poses of the hand-object system with friction (the objects are supported on the table surface) and without friction (the hand-object system is elevated by the robot arm). The effect of kinetic friction force for the lightweight plastic strawberry (18 g) is insignificant (the maximum reconfiguration increases from 22 mm to 23 mm without friction), while for the heavy bottle of mustard (600 g) the friction effect is significant (the maximum reconfiguration increases from 38 mm to 44 mm without friction).

D. Accompanying Video

All the simulated and experimental paradigms conducted with the model and the everyday life objects are included in an HD quality video in [37]. During the experiments, the parasitic object motion compensation is not perfect, due to the limited precision of the Barrett WAM robot arm and due to the aforementioned friction phenomena and the possible asymmetries (e.g., tendon routing asymmetries) in the robot hand structure. Another factor that causes the shaking of the object is that we use large contact forces (we do not employ the grasping force optimization results), in order to maximize the imposed parasitic object displacements and make the robot arm compensatory motions more evident.

IV. Conclusion

In this paper, we presented a methodology based on constrained optimization methods, which derives stable, minimal effort grasps for adaptive, compliant, and underactuated robot

hands, estimates the post-contact parasitic object motions, and derives appropriate robot arm trajectories that eliminate these parasitic motions, facilitating grasp stabilization. The methodology takes advantage of models that describe the kinematics of adaptive robot hands, even when they are implemented with complex and hard-to-model flexure joints, and deals with both symmetric and nonsymmetric grasps. The parasitic object motions have been shown to depend on the hand and object parameters, the contact forces exerted through the robot fingertips, and the kinetic friction force that resists the reconfiguration of the hand-object system. The accuracy of the proposed methods was experimentally validated through extensive simulated and experimental paradigms, involving a redundant seven DoF robot arm (Barrett WAM) and different, adaptive, compliant, and underactuated robot hands (Yale OpenHand models T42PP, T42PF, and T42FF). We feel that deriving stable, minimal effort grasps and compensating for possible parasitic object motions is a prerequisite of paramount importance for many practical grasping and in-hand manipulation tasks with underactuated hands.

While this paper represents a good initial step in this area, a number of follow-up efforts should be performed. First, while the framework presented applies also to 3-D motions, only planar hands and movements were examined in the experimental results shown here. In this respect, we plan to extend this paper and investigate the accuracy of the proposed methodology for predicting the parasitic object motions in 3-D space and eliminating them with appropriate compensatory motions of the robot arm. To do so, we plan to use other multifingered hands of the OpenHand project (e.g., Model O). Other future plans or ours, are the investigation of the roles of object weight and gravity in the execution of 3-D tasks and the extension of the proposed methods for complex objects with known geometry.

ACKNOWLEDGMENT

The authors would like to thank R. R. Ma and A. Nawroj for their helpful discussions related to the work presented in this paper.

REFERENCES

[1] A. M. Dollar and R. D. Howe, "A robust compliant grasper via shape deposition manufacturing," *IEEE/ASME Trans. Mechatron.*, vol. 11, no. 2, pp. 154–161, Apr. 2006.

[2] D. M. Aukes *et al.*, "Design and testing of a selectively compliant underactuated hand," *Int. J. Robot. Res.*, vol. 33, pp. 721–735, Feb. 2014.

[3] L. U. Odhner *et al.*, "A compliant, underactuated hand for robust manipulation," *Int. J. Robot. Res.*, vol. 33, no. 5, pp. 736–752, Apr. 2014.

[4] R. R. Ma, L. U. Odhner, and A. M. Dollar, "A modular, open-source 3D printed underactuated hand," in *Proc. IEEE Int. Conf. Robot. Autom.*, May 2013, pp. 2737–2743.

[5] A. G. Zisimatos, M. V. Liarokapis, C. I. Mavrogiannis, and K. J. Kyriakopoulos, "Open-source, affordable, modular, light-weight, underactuated robot hands," in *Proc. IEEE/RSJ Int. Conf. Intell. Robot. Syst.*, Sep. 2014, pp. 3207–3212.

[6] R. Deimel and O. Brock, "A novel type of compliant and underactuated robotic hand for dexterous grasping," *Int. J. Robot. Res.*, vol. 35, no. 1–3, pp. 161–185, 2016.

[7] M. Ciocarlie *et al.*, "The Velo gripper: A versatile single-actuator design for enveloping, parallel and fingertip grasps," *Int. J. Robot. Res.*, vol. 33, no. 5, pp. 753–767, 2014.

[8] L. U. Odhner, R. R. Ma, and A. M. Dollar, "Precision grasping and manipulation of small objects from flat surfaces using underactuated fingers," in *Proc. IEEE Int. Conf. Robot. Autom.*, May 2012, pp. 2830–2835.

[9] R. R. Ma and A. M. Dollar, "An underactuated hand for efficient finger-gaiting-based dexterous manipulation," in *Proc. IEEE Int. Conf. Robot. Biomimetics (ROBIO)*, Dec. 2014, pp. 2214–2219.

[10] A. Bicchi and A. Marigo, "Dexterous grippers: Putting nonholonomy to work for fine manipulation," *Int. J. Robot. Res.*, vol. 21, nos. 5–6, pp. 427–442, 2002.

[11] M. Gabiccini, E. Farnioli, and A. Bicchi, "Grasp and manipulation analysis for synergistic underactuated hands under general loading conditions," in *Proc. IEEE Int. Conf. Robot. Autom.*, May 2012, pp. 2836–2842.

[12] C. I. Mavrogiannis, C. P. Bechlioulis, M. V. Liarokapis, and K. J. Kyriakopoulos, "Task-specific grasp selection for underactuated hands," in *Proc. IEEE Int. Conf. Robot. Autom.*, Jun. 2014, pp. 3676–3681.

[13] A. Bicchi, M. Gabiccini, and M. Santello, "Modelling natural and artificial hands with synergies," *Philos. Trans. Roy. Soc. B, Biol. Sci.*, vol. 366, no. 1581, pp. 3153–3161, Nov. 2011.

[14] M. Roa and R. Suárez, "Grasp quality measures: Review and performance," *Auto. Robots*, vol. 38, no. 1, pp. 65–88, 2015.

[15] S. L. Chiu, "Task compatibility of manipulator postures," *Int. J. Robot. Res.*, vol. 7, no. 5, pp. 13–21, 1988.

[16] M. Ciocarlie and P. Allen, "A constrained optimization framework for compliant underactuated grasping," *Mech. Sci.*, vol. 2, no. 1, pp. 17–26, 2011.

[17] M. Ciocarlie and P. Allen, "Data-driven optimization for underactuated robotic hands," in *Proc. IEEE Int. Conf. Robot. Autom.*, May 2010, pp. 1292–1299.

[18] Y. Su, Y. Wu, K. Lee, Z. Du, and Y. Demiris, "Robust grasping for an under-actuated anthropomorphic hand under object position uncertainty," in *Proc. IEEE-RAS Int. Conf. Humanoid Robots*, Nov. 2012, pp. 719–725.

[19] Z. Chen *et al.*, "An adaptive compliant multi-finger approach-to-grasp strategy for objects with position uncertainties," in *Proc. IEEE Int. Conf. Robot. Autom. (ICRA)*, May 2015, pp. 4911–4918.

[20] D. Prattichizzo, M. Malvezzi, M. Aggravi, and T. Wimböck, "Object motion-decoupled internal force control for a compliant multifingered hand," in *Proc. IEEE Int. Conf. Robot. Autom.*, May 2012, pp. 1508–1513.

[21] M. Malvezzi and D. Prattichizzo, "Internal force control with no object motion in compliant robotic grasps," in *Proc. IEEE/RSJ Int. Conf. Intell. Robots Syst. (IROS)*, Sep. 2011, pp. 1008–1014.

[22] M. V. Liarokapis and A. M. Dollar, "Post-contact, in-hand object motion compensation for compliant and underactuated hands," in *Proc. IEEE Int. Symp. Robot Human Interact. Commun. (RO-MAN)*, Aug. 2016, pp. 986–993.

[23] M. V. Liarokapis, A. M. Dollar, and K. J. Kyriakopoulos, "Humanlike, task-specific reaching and grasping with redundant arms and low-complexity hands," in *Proc. Int. Conf. Adv. Robot. (ICAR)*, Jul. 2015, pp. 490–497.

[24] L. U. Odhner and A. M. Dollar, "The smooth curvature model: An efficient representation of Euler–Bernoulli flexures as robot joints," *IEEE Trans. Robot.*, vol. 28, no. 4, pp. 761–772, Aug. 2012, doi: 10.1109/TRO.2012.2193232

[25] D. Prattichizzo and J. C. Trinkle, "Grasping," in *Springer Handbook of Robotics*. B. Siciliano and O. Khatib, Eds. Berlin, Germany: Springer-Verlag, 2008, pp. 671–700.

[26] M. Gabiccini, A. Bicchi, D. Prattichizzo, and M. Malvezzi, "On the role of hand synergies in the optimal choice of grasping forces," *Auto. Robots*, vol. 31, pp. 235–252, Oct. 2011.

[27] M. R. Cutkosky and I. Kao, "Computing and controlling compliance of a robotic hand," *IEEE Trans. Robot. Autom.*, vol. 5, no. 2, pp. 151–165, Feb. 1989.

[28] L. U. Odhner and A. M. Dollar, "The smooth curvature flexure model: An accurate, low-dimensional approach for robot analysis," in *Proc. Robot.: Sci. Syst.*, 2010, pp. 137–144.

[29] L. U. Odhner and A. M. Dollar, "Stable, open-loop precision manipulation with underactuated hands," *Int. J. Robot. Res.*, vol. 34, no. 11, pp. 1347–1360, 2015.

[30] M. Malvezzi, G. Gioioso, G. Salvietti, D. Prattichizzo, and A. Bicchi, "SynGrasp: A MATLAB toolbox for grasp analysis of human and robotic hands," in *Proc. IEEE Int. Conf. Robot. Autom. (ICRA)*, May 2013, pp. 1088–1093.

[31] P. I. Corke, "A robotics toolbox for MATLAB," *IEEE Robot. Autom. Mag.*, vol. 3, no. 1, pp. 24–32, Mar. 1996.
[32] B. Rooks, "The harmonious robot," *Ind. Robot, Int. J.*, vol. 33, no. 2, pp. 125–130, 2006.
[33] *Yale OpenHand Project*, accessed on Nov. 29, 2016. [Online]. Available: http://www.eng.yale.edu/grablab/openhand
[34] L. P. Jentoft, Y. Tenzer, D. Vogt, R. J. Wood, and R. D. Howe, "Flexible, stretchable tactile arrays from MEMS barometers," in *Proc. 16th Int. Conf. Adv. Robot.*, 2013, pp. 1–6.
[35] B. C. Calli *et al.*, "Benchmarking in manipulation research: The YCB object and model set and benchmarking protocols," *IEEE Robot. Autom. Mag.*, vol. 22, no. 3, pp. 36–52, Mar. 2015.
[36] H. G. Howell, "The general case of friction of a string round a cylinder," *J. Textile Inst. Trans.*, vol. 44, nos. 8–9, pp. 359–362, 1953.
[37] *Post-Contact, In-Hand Object Motion Compensation with Adaptive Hands: Video*, accessed on Nov. 29, 2016. [Online]. Available: https://www.youtube.com/watch?v=dmcEUc17Lrw
[38] *RightHand Robotics Labs*, accessed on Nov. 29, 2016. [Online]. Available: http://www.labs.righthandrobotics.com/

Minas V. Liarokapis (S'09–M'14) received the Diploma in computer engineering from the University of Patras, Patras, Greece, the M.Sc. degree in information technologies in medicine and biology from the National Kapodistrian University of Athens, Athens, Greece, and the Ph.D. degree in mechanical engineering from the National Technical University of Athens, Athens.

He is currently a Post-Doctoral Associate with the GRAB Laboratory, Department of Mechanical Engineering and Materials Science, Yale University, New Haven, CT, USA. His current research interests include robot grasping and manipulation, human robot interaction, robot hands design, noninvasive brain machine interfaces, and machine learning and pattern recognition.

Aaron M. Dollar (S'02–M'07–SM'13) received the B.S. degree in mechanical engineering from the University of Massachusetts at Amherst, Amherst, MA, USA, and the Ph.D. degree in engineering sciences from Harvard University, Cambridge, MA, USA.

He was a Post-Doctoral Researcher for two years at the MIT Media Laboratory, Massachusetts Institute of Technology, Cambridge. He is currently the John J. Lee Associate Professor of Mechanical Engineering and Materials Science with Yale University, New Haven, CT, USA. His current research interests include human and robotic grasping and dexterous manipulation, mechanisms and machine design, and assistive and rehabilitation devices including upper-limb prosthetics and lower-limb orthoses.

Dr. Dollar was a recipient of the 2013 DARPA Young Faculty Award, the 2011 AFOSR Young Investigator Award, the 2010 Technology Review TR35 Young Innovator Award, and the 2010 U.S. National Science Foundation CAREER Award.